Cavity detection using microgravity in a highly urbanized setting: A case study from Reims, France

Thomas Jacob, P. Pannet, F. Beaubois, Jean-Michel Baltassat, Y. Hannion

Cavity detection using microgravity in a highly urbanized setting: a case study from Reims, France

Jacob, T.[a], Pannet, P.[b], Beaubois, F. [a], Baltassat, J.M. [a], Hannion, Y.[c]

[a]**BRGM,** 3 avenue Claude Guillemin BP36009, 45060 Orléans Cedex 2, France

[b]**BRGM,** Arteparc Bâtiment A, 2 rue des Peupliers 59810 Lesquin, France

[c]**BRGM,** Pôle technologique Henri Farman, 12 rue Clément Ader, 51100 Reims, France

Accepted Received in original form

Corresponding author: Thomas Jacob**,** BRGM 3 avenue Claude Guillemin BP36009, 45060 Orléans Cedex 2, France

e-mail: t.jacob@brgm.fr, Tel: 33 (0) 2 38 64 37 40

Highlights

- Microgravity surveying for cavity detection in a highly urbanized city centre
- A successful correction scheme for buildings and underground structures is presented
- Drill holes within gravity anomalies discovered a two- level cellar

Abstract

In this study, we present a microgravity survey carried out in a highly urbanized city centre setting in Reims, France, with the aim of detecting undocumented cavities below ground. The occurrence of two ground collapses affecting a busy street, linked to ill-filled cellars, motivated this survey. In this context, surrounding buildings and underground structures, such as existing cellars or parking lots, constitute respectively excess mass above, and deficit mass below the gravimeter, which result in negative gravity anomalies. These anomalies may have magnitudes comparable to or larger than the target signal, hence obscuring its detection.

We present a correction scheme for buildings and underground structures, which is effective, as evidenced by the mitigation of important border anomalies present in the uncorrected Bouguer anomaly and no longer visible in the corrected Bouguer anomaly. In effect, these corrections make the Bouguer anomaly more straightforward to interpret, which facilitates the determination of a regional anomaly, and ultimately leads to a more meaningful residual anomaly. We also present an error budget estimate, in which errors in the anthropogenic corrections are approximated. This allows us to establish a significance threshold, which is used to delineate significant anomalies.

A number of significant anomalies were found, and drillholes were recommended to control the anomalies and check for cavities. A two-level cellar was found in the middle of City Hall Plaza, within a major gravity anomaly. Other drill holes found un-compacted fill material.

Keywords: gravity survey; cavity detection; gravity corrections
Declarations of interest: none

1. Introduction

Within 11 days of June 2016, two ground collapses, located less than 10 m apart, occurred in a busy downtown street of Reims, France. These collapses were some 3 m deep, and some 5 m by 3 m in footprint (Figure 1). Notably, the collapses occurred after an especially rainy period, which may have helped trigger them. The collapses were linked with ill-filled cellars from before World War I.

Local authorities commissioned BRGM (Bureau de Recherches Géologiques et Minières), the French geological survey, to detect other such cavities in the surrounding streets, to assess and mitigate the collapse hazard.

Within this scope, local authorities commissioned BRGM to carry out a microgravity survey, comprising 680 stations. This method is well suited to detect underground cavities, both natural (Butler, 1984; Leucci and De Giorgi, 2010; Martínez-Moreno et al., 2013; Mochales et al., 2008; Omnes, 1977), and anthropogenic (Bishop et al., 1997; Fais et al., 2015; Fajklewicz, 1976; Martinez-Moreno et al., 2016; Styles et al., 2006). Indeed, the microgravity method allows measuring minute local gravity anomalies linked to density contrasts below ground. A cavity can be associated with a mass deficit, or negative density contrast below ground, which generates a negative gravity anomaly.

In urban settings, surrounding buildings constitute excess mass above the gravity meter, leading to an upward attraction which decreases the gravity value, and these effects need to be corrected (Blížkovský, 1979; Debeglia and Dupont, 2002; Nowell, 1999; Radogna et al., 2003). Likewise, surrounding underground voids (cellars, underground parking lots, basements…), locally decrease the gravity value, and need to be corrected (Debeglia and Dupont, 2002; Nowell, 1999). Both of these effects, if not accounted for, may mask the gravity anomalies from target unknown cavities; as their amplitude may exceed that of the target anomalies (Debeglia and Dupont, 2002).

To correct for these effects as accurately as possible, one needs the precise 3D geometry of surrounding buildings and voids and their respective densities (Chromčák et al., 2016; Panisova et al., 2012). This is especially true for gravity measurements made within complex historical religious buildings, where photogrammetry or laser scanning may be used to render the 3D geometry of the buildings and underground structures (Panisova et al., 2013; Panisova et al., 2016; Panisova et al., 2012). This is

however not readily applicable to large scale urban surveys, wherein gravity stations may be adjacent to hundreds of buildings, and as many underground structures, for evident time and cost reasons.

There are few examples of gravity surveys in highly urbanized settings such as city centres in the literature. In these studies, the buildings are corrected for using prisms representing the buildings as a whole, having equivalent bulk densities (Dilalos et al., 2018; Yu, 2014), or a set of prisms which account for the internal building structure (outer walls, floor slabs, roof…) (Castiello et al., 2010; Chromčák et al., 2016; Styles et al., 2006).

In both cases, the equivalent bulk densities, the internal building structure and the densities of its constitutive elements must be determined accurately. These tasks are not trivial, as is recently shown by Loj and Porzucek (2019) . These authors compare the gravity effects of various building types modelled as both bulk density prisms and as prisms accounting for the internal structure. They find that the difference between the two modelling schemes is in the range of 7 to 14 µgals for the stations closest to the buildings, and that the equivalent bulk density should be estimated to within ±0.04 g/cm^3 for best results.

Here, we present a microgravity survey case study for cavity detection in a highly urbanized downtown area of Reims, France. We first present the study area, the survey acquisition and processing, with an emphasis on building and existing underground structure corrections, and detail a methodology for these corrections. The gravity anomalies are then presented and discussed, along with an assessment of the error budget and the significance threshold of the anomalies. The outcome of the study in terms of drill holes and discovered cavities are presented.

2. Material and Methods

2.1 Site description

The city of Reims, located in the Northeast of France (Figure 1a), is built upon Upper Cretaceous Chalk of the Campanian. Over millennia of settlement since before Roman times, hundreds of underground cavities have been excavated in the soft chalk, with networks of underground caves, tunnels, and chalk

mines crisscrossing the city (Thuon, 2010). The most famously known today are the ones used by champagne makers to mature and store their produce.

Furthermore, the city of Reims was largely destroyed during the First World War, and the following reconstruction in the 1920s did not follow the pre-war street plan. New streets were built where building blocks once stood before the Great War. Cellars and underground cavities underneath the former building blocks were often hastily filled, leading to a significant collapse hazard a century later (Thuon, 2010).

Several meters of sandy to rubble fill are located above the chalk.

The two ground collapses occurred on the 8th and on the 19th of June 2016, in a busy downtown street in the vicinity of Reims City Hall (Figure 1). The collapses were linked to the roof collapse of ill-filled cellars from before the Great War (Vilain, 2016), now located in the middle of a street, because of the street plan changes during reconstruction. The collapses are located in immediate vicinity from one another and have footprints larger than 5 m by 3 m.

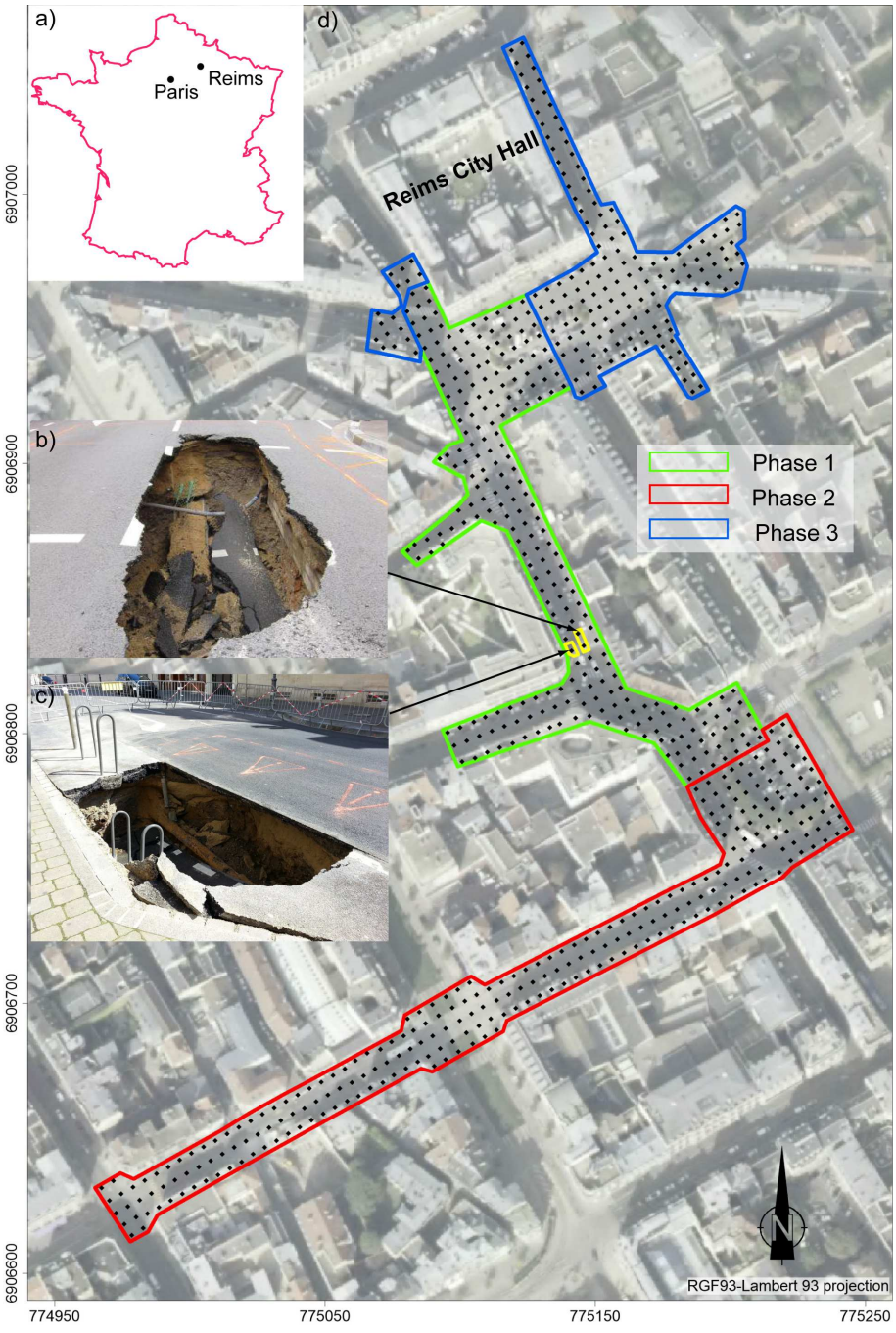

Figure 1a: general location map of Reims in France, b) photograph of the first collapse, (© l'Union) c) photograph of the second collapse (© Radio France - Philippe Rey-Gorez) d) location map of gravity survey (black diamonds: gravity stations) showing the three survey phases. The yellow polygons are the collapse footprints.

2.2 Gravity survey characteristics

In total, 680 gravity stations were acquired at a 5 m spacing. This station spacing was chosen because it allows to detect the gravity signal from typical cavities in this area, which are cellars having footprints larger than 6 m x 3 m, heights between 2 and 3 m, and roof depths no greater than 3 to 5 m (Thuon, 2010). We however acknowledge that smaller cavities may not be detected using this station spacing.

The study was conducted in three separate phases (Figure 1 and Table 1), between June and December 2016, following a planning decided by the City of Reims. During each phase, gravity measurements were made during daytime, and car traffic was cut off over the survey area and rerouted to insure optimal conditions for the measurements. Indeed, gravity acquisition is sensitive to environmental ambient noise levels, which, in urban areas, are generated by nearby car traffic. Pedestrian traffic was however not cut off, and curious onlookers as well as pedestrians were a noise source, as they walked close to the meter while it was measuring. For a review of environmental noise sources and means to filter them, please refer to Boddice et al. (2018).

Phase	Dates	Number of stations	Number of repeat measurements	Meter used	1 sigma repeat error (mGal)
1	28/06/2016-02/07/2016	257	71	Scintrex CG-3 M # 403245	0.011 mGal
2	07/11/2016-10/11/2016	257	58	Scintrex CG-5 # 40172	0.007 mGal
3	05/12/2016-06/12/2016	166	42	Scintrex CG-5# 40539	0.004 mGal

Table 1: Survey characteristics.

A different gravity meter was used during each survey phase (Table 1). A calibration factor of 1.00000 was used for each meter, as the gravity changes measured within each survey were smaller than 1 mGal, due to the relatively flat topography on site. Indeed, first order gravity changes are dominated by station height changes.

Two base stations were used throughout the survey – one for phases 1 and 3, and one for phase 2. The two base stations were tied to one another with three back and forth measurements, with a standard deviation of 0.003 mGal for the three gravity determinations between the two base stations.

Loop duration, the timespan between return measurements at the base station to assess instrumental drift, did not exceed 1 h. At each station, gravity readings consisted of at least one 60 s measurement, and further readings were measured if instrument tilt were larger than ±10 arcsec, or if the standard

deviation of a given measurement cycle rose due to local ambient noise (i.e. when a pedestrian walked by too close). Gravity readings at the base station consisted of five 60s measurements. The percentage of repeat measurements, i.e. gravity stations measured at least twice in independent loops, is respectively 27.6 %, 22.5 % and 27.6 %, for phases 1, 2 and 3. In this manner, statistics can be determined on the repeat measurements, to determine the reproducibility of the data for a given survey. For each survey, the gravity repeat measurements follow a zero-mean Gaussian distribution with a standard deviation no higher than 0.011 mGal for phase 1, and as low as 0.004 mGal for phase 3 (Table 1). The difference in repeat error between the meters may in part be due to varying ambient noise levels during the different phases of the survey, but also to the intrinsic measurement quality of each gravity meter used (Table 1). Indeed, each meter reacts differently to the so-called hysteresis or relaxation effect after transport (Flury et al., 2007; Repanić and Kuhar, 2018), and to temperature changes (Fores et al., 2017) and tilt during storage or transport effects (Reudink et al., 2014), all of which negatively impact measurement precision. These effects tend to get worse with time and usage, leading to the meter needing service by the manufacturer on a regular basis (every ~2 years, in our experience).

Additional quality control consisted in targeted repeat measurements on dubious stations, as detected on the preliminary Bouguer map computed after each workday.

Relative station elevations and positions were determined using a total station (Trimble S7), with loop closures inferior to 0.01 m. To reference the stations' positions in the RGF93-Lambert 93 spatial reference, a differential GPS rover (Trimble Geo 7X with Zephyr II antenna) post-processed against a GPS base station located less than 20 km away was used. The absolute positions of select topographical base stations with a precision of 0.01 cm in the (X,Y) plane and 0.02 cm in the Z direction were determined.

2.3 Gravity data processing

2.3.1 Bouguer anomaly

The data were processed to remove all usual gravity effects needed to obtain the Bouguer anomaly:

- The effects of solid earth tides on gravity were corrected for using the tide corrections within the meters' software, based on Longman (1959) . Although this tidal correction is not up to the

standards of modern earth tide corrections, any uncorrected tidal effects are effectively accounted for and corrected within the hourly drift estimate. The same applies to ocean tidal loading and atmospheric effects, which are not explicitly corrected for, but are accounted for in the hourly drift estimate.

- Instrument drift was assumed linear and evaluated using the opening and closing base station measurements of each survey loop, one drift value is thus obtained for each loop, and is used to correct the measured stations within each loop.
- The normal gravity value based on the GRS 80 (Moritz, 1980) geodetic system constants using Somigliana's formula was corrected for,
- Free-air and simple Bouguer correction were performed,
- Terrain corrections were computed using a 1 m x 1m spacing airborne LIDAR DEM, the RGE Alti® product from IGN. Terrain in the surrounding 30 m of each station was considered for the correction, and corrected for using a flat topped square prism formulation (Nagy, 1966). Due to the smooth topography with no ruggedness, terrain corrections reach at most 0.003 mGal, for a terrain density of 2 g/cm^3, a typical value for the uppermost compact fill material. Terrain corrections further than 30 m away from each station were not computed because i) the resulting signal is likely to be of small magnitude due to the flat and smooth topography of the region, and ii) this signal will be a long wavelength signal. Because the computed regional anomaly accounts for long-wavelength signal (see section 2.3.3), these uncorrected terrain correction effects should be captured within the regional anomaly, resulting in a residual anomaly having mostly short wavelength signal related to the targeted shallow cavities.
- The density value chosen for the reduction is 2 g/cm^3, as this is a typical value for the uppermost compact fill material.

These corrections lead to the classical Bouguer anomaly (Figure 2), wherein the effects of nearby buildings and underground structures are evident, and need to be corrected for.

Gridding of the Bouguer anomaly was performed using a bicubic interpolation algorithm (D'Errico, 2005; Jamal, 2014), using a smoothing factor of 0.0005.

2.3.2 Anthropogenic corrections: building and underground structure corrections

Ideally, one should model the 3D density distribution of buildings as accurately as possible to obtain the most precise building corrections. This necessitates knowledge of the 3D volume of the building, and the densities of its constitutive elements. For small-scale studies involving a limited number of buildings, and in cases where the stations are located within the buildings, the use of geodetic techniques such as photogrammetry to render the 3D structure of the buildings is highly recommended (Panisova et al., 2016; Panisova et al., 2012).

In our study, more than 150 buildings are adjacent to the gravity stations, which precludes their precise 3D rendering by geodetic methods for cost and time considerations. Furthermore, all of our stations are located on the streets, at a distance greater than 1 m from neighbouring walls or underground structures, and not within the buildings.

Some authors approximate the buildings as prisms with equivalent bulk densities (Dilalos et al., 2018; Yu, 2014), while others model the building structural elements as prisms (Castiello et al., 2010; Debeglia and Dupont, 2002; Radogna et al., 2003; Styles et al., 2006). Here, we opt for the second option, with a variant.

We model the building outer walls as a series of vertical line masses with a 0.1 m spacing, having linear densities determined by the wall thickness and the wall mean density (see Bott (1959) for the formula of the attraction of vertical line masses). The rationale for this methodology is to account for changes in wall height due to slopping streets, which a single right rectangular prism cannot account for. The line masses are located within the centre of the walls' thickness. We chose a spacing of 0.1 m because this leads to negligible differences in attraction, < 0.001 mGal, compared to the attraction of a 'full' wall, modelled as a prism, for stations at 1 m distance from the walls. This difference decreases as the distance from the wall increases, and no single station in this study is located closer to 1 m from any surrounding wall.

We make the following simplifications: windows and doors are not included in the model (i.e. the walls are full), nor are floor slabs or roofs included. We therefore consider the building mass to be

concentrated on the periphery of the building, in contrast to the equivalent bulk density approach, which considers building mass to be evenly distributed within the building. The building architecture style on the study site is mostly post World War I 1920's reconstruction buildings, with thick limestone, brick and plaster outer walls and beams and floor slabs made of wood. In such building architecture style, most of the building mass is concentrated on the outer walls of the building, as the wooden floor slabs and beams are less dense and less thick than the outer walls. For modern buildings, this approximation may not hold true as most of the mass may be concentrated within reinforced concrete floor slabs, which are thicker than the exterior paving slabs.

Using the methodology above described, data needed to correct for buildings are building height, measured using the total station or a laser rangefinder in the field, building footprint, given by the national French cadastre (BD Parcellaire ®, IGN), building wall thickness, measured in the field using a measuring tape, and building wall density. Building mean wall density was set to 2 g/cm^3, as building walls are made of limestone on the outside, and brick and plaster on the inside.

Whenever the owners granted access, cellars, caves and other underground structures were visited and their dimensions and orientations were measured with a laser rangefinder and a compass. In some cases, the ground plans of the underground structures were accessible and used. In a limited number of cases, the dimensions of existing underground cavities could not be obtained because no access was granted to the building. Therefore, not every single known underground structure is modelled and corrected for, hence leading to residual anomalies due to these uncorrected cavities (see section 3.6).

Underground cavities were corrected for using a polygonal flattop prism formulation (Murthy and Swamy, 1996). A density contrast of -1.7 g/cm^3 between the cavities and surrounding chalk was used. This value comes from the estimated bulk density of the Campanian chalk, having a 42 % porosity (Moreau, 2008), and considering a 25% water saturation.

Buildings and known underground cavities are corrected for within the surrounding 50 m from each station. This limit was chosen because both building corrections and underground structure corrections from a single building and cavity are negligible at that distance (i.e. <0.001 mGal), given the typical building dimensions and underground structure dimensions in the study area. This distance must

however be adjusted with respect to building height on the study area, and increased when high-rise buildings are located close-by, as these have an non-negligible effect at a distance greater than 50 m (see for eg. (Dilalos et al., 2018; Yu, 2014))

Furthermore, the cumulative effects of uncorrected buildings located further than 50 m away from each station is most likely a longer-wavelength signal. In the present microgravity study, where the target signal is likely short-wavelength due to shallow voids, the uncorrected building long-wavelength signal will be incorporated within the regional anomaly, and therefore accounted for.

The anthropogenic correction map is shown in Figure 3, and is commented in section 3.2.

Adding these corrections to the classical Bouguer anomaly leads to the complete Bouguer anomaly (Figure 4).

2.3.3 Regional and residual anomaly

Separation of the Bouguer anomaly into regional and residual components is done by surface fitting using a gridding algorithm provided by Jamal (2014), and based on D'Errico (2005). Using this algorithm, the regional anomaly (Figure 5) is evaluated and controlled by a smoothing factor, which was chosen so that the regional anomaly correctly accounts for the long-wavelength components of the Bouguer anomaly, i.e., a North-South long wavelength gradation, with lower values to the South and higher values to the North. The smoothing factor used to determine the regional anomaly is 0.01.

The regional anomaly should account for the effects of the deeper regional geological setting, and not that of the sub-surface, which is highlighted in the residual anomaly. Given the very limited study area length scale, 500 m by 300 m, and given the tabular nature of sedimentary layers in the area and absence of major tectonic features, the regional anomaly from deeper geology is expected to be quasi-planar.

However, long-wavelength and gradual sub-surface density changes occurring over the study area, such as one that might occur with a gradually varying thickness of denser fill overlying the low density chalk, may also generate long-wavelength signal at the survey scale, which may be captured within the regional anomaly.

Subtraction of the regional anomaly from the Bouguer anomaly yields the residual anomaly, which is representative of the short-wavelength density distribution in the sub-surface (Figure 7), which we interpret in section 3.6.

3. Results

3.1 Classical Bouguer Anomaly

The Bouguer anomaly map without anthropogenic corrections, i.e. the classical Bouguer Anomaly, is presented in Figure 2, for a density reduction of 2 g/cm^3.

Immediately evident in this map are the large negative anomalies surrounding two buildings located in the centre of the study area (X=775100 m, Y =6906850 m), and to the North (X=775150 m, Y = 690700 m). The first building has a four-level underground parking lot, and the second building a three-level cellar complex. These major anomalies are likely due to the gravity effects of these massive underground structures. Moreover, over the entire study area, negative anomalies develop towards the surrounding buildings, making the map difficult to interpret. This clearly shows that anthropogenic corrections need to be applied and are critical to obtain an interpretable Bouguer anomaly map.

Figure 2: Bouguer anomaly (mGal), for a reduction density of 2 g/cm^3, without anthropogenic corrections. Iso-contours are every 0.02 mGal. Modelled underground structures are represented by green polygons, and modelled buildings by blue polygons.

3.2 Building and underground structure corrections

The building and underground structure correction map is presented in Figure 3. The values of these corrections are positive, as the bulk of the building mass, which constitute positive density contrast, lie

above the stations, and the underground structures, which have a negative density contrast, lie below the stations. In uncommon cases in which a cavity lies above a gravity station, the correction is negative (Debeglia & Dupont, 2002). The values of the corrections range between 0.008 mGal to 0.190 mGal, the lower values affect stations located further away from buildings and underground voids, the higher values of the corrections affect stations located closer to the buildings and underground structures. The highest values are reached in the surrounding vicinity of the four level underground parking lot located in the centre of the study area, and in the vicinity of the three level cellar complex at the North of the study area.

Adding the anthropogenic corrections to the classical Bouguer anomaly leads to the complete Bouguer anomaly.

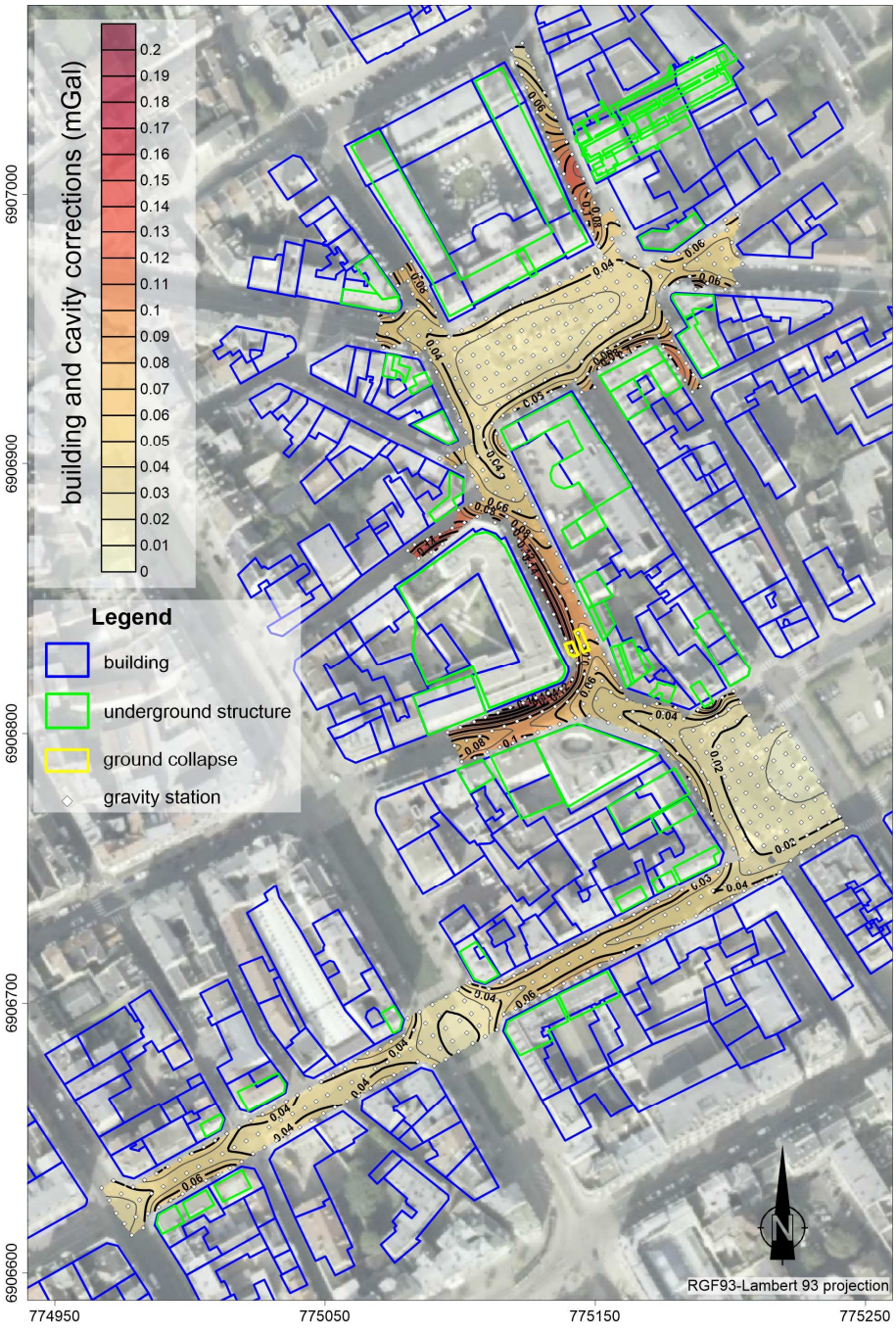

Figure 3: Building and underground structure corrections (mGal)

3.3 Complete Bouguer anomaly and regional anomaly map

The complete Bouguer anomaly is presented in Figure 4. The dominant anomalies observed on the classical Bouguer anomaly (Figure 2) are no longer visible, a testament that the building and underground structure corrections (Figure 3) are effective. Consequently, the range on the complete Bouguer anomaly, 0.120 mGal, is much reduced compared to that of the classical Bouguer anomaly,

1 0.230 mGal, making its interpretation an easier task. Indeed, identifying anomalies of interest, not those
2 due to nearby buildings and underground structures, and assessing an adequate regional anomaly, is now
3 a more straightforward task than with the classical Bouguer anomaly, which is highly distorted by the
4 uncorrected building and underground structure effects.
5 The complete Bouguer anomaly map exhibits higher values to the North of the study area, and lower
6 values to the South. Local anomalies are readily observed, such as the one visible on the City Hall plaza,
7 and immediately to the North of the collapsed zone.
8 The regional anomaly is show in Figure 5 (see section 2.3.3 for details), and it adequately renders the
9 long wavelength component of the Bouguer anomaly.
10

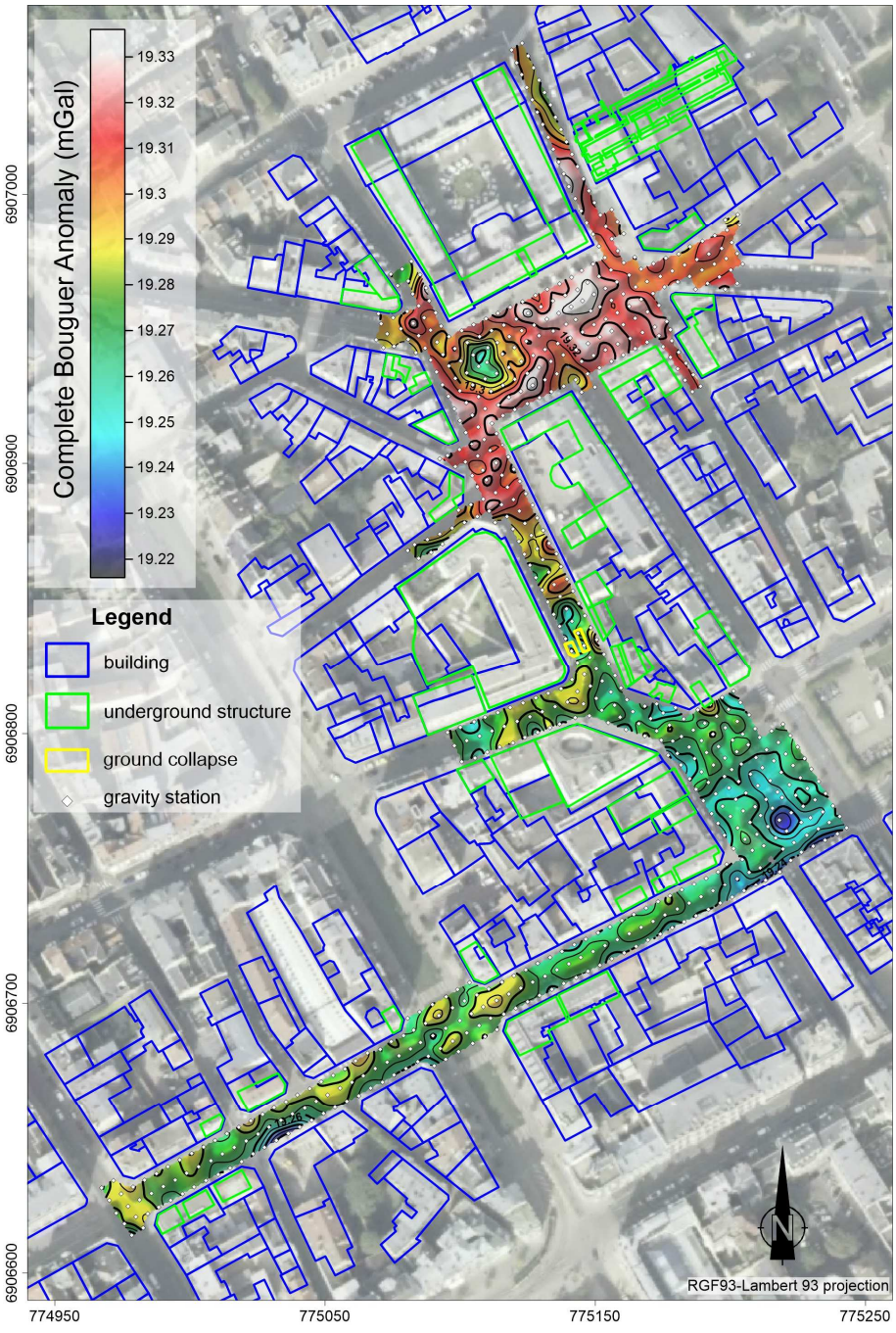

Figure 4: Complete Bouguer Anomaly (mGal). Isocontours are every 0.01 mGal.

Figure 5: Regional anomaly map (mGal)

3.4 Bouguer anomaly error estimate

It is good practice to evaluate the error on the Bouguer anomaly, in order to assess which anomalies are significant. Following Debeglia & Dupont (2002), the error on the Bouguer anomaly e_{BA} is evaluated as the quadratic sum of its constitutive elements:

$$e_{BA} = \sqrt{e_g^2 + e_z^2 + e_{TC}^2 + e_{AC}^2} \quad \text{(eq. 1)}$$

With e_g the error on the gravity measurement, given by the standard deviation of the gravity repeat measurements (Table 1), e_z the error on the elevation correction, where 0.01 m elevation error equates to 0.002 mGal error for a density of 2 g/cm^3. e_{TC} and e_{AC} are the errors on the terrain corrections and on the anthropogenic corrections – i.e building and underground structure corrections, which we consider to be station-dependent, linearly related to the magnitude of the correction at each station.

For station *i*, the error on the anthropogenic correction is approximated as:

$$\left(e_{AC}\right)_i = \alpha(AC_i - \min(AC)) \quad \text{(eq. 2)}$$

Where α is factor set to 0.2, AC_i is the anthropogenic correction value for station i, and $\min(AC)$ is the minimum correction value of the dataset. We follow strictly the same methodology for the terrain corrections. In effect, this means that stations with minimal TC or AC values will have minimal errors - this is the case for stations located far from buildings, known caves, or rugged topography (Figure 3). Conversely, stations with highest TC or AC values will have the highest errors; these are stations closest to buildings, known cavities and rugged topography (Figure 3).

Our working hypothesis is that correction errors stemming from ill-modelled cavities, ill-modelled buildings, or ill-modelled topography, will be highest when the correction value is highest – i.e. when the station is closest to the causative sources, and that conversely, it will be lower when the correction value is lower, when the stations are further away from the causative sources. This is a consequence of the strong distance dependence of the gravity signal between station and source, and is discussed in Debeglia & Dupont (2002).

Corrections errors stemming from ill-modelled cavities are due to errors in cavity dimensions, depth, location, density contrast, and to the flattop prism approximation used in this study (see section 2.3.2), when the cavity does not have a flat ceiling. Corrections errors stemming from ill-modelled buildings are due to errors in building dimensions, location, wall thickness, assigned densities, and to errors stemming from the building correction methodology, which concentrates mass on the outer building walls, without considering windows, doors, floor slabs or roofs (see section 2.3.2).

Correction errors stemming from ill-modelled topography comes from the digital elevation model precision and spacing. In this study, these errors are small, as topography on site is mostly flat or gently sloping, with no marked ruggedness, and a high precision 1m LIDAR DEM is used.

By assigning α to 0.2, we consider a 20 % error on the range of the corrections (TC or AC), although we acknowledge that this number may in reality be distance-dependent to the causative source. We consider that the chosen value for α, 0.2, to be conservative, although further modelling should be performed to assess this factor more precisely, yet this is outside of the scope of the present paper.

The error on the Bouguer anomaly, while not presented in a figure, mimics that of the significance threshold (Figure 6, next section), by a factor of two. The error on the Bouguer anomaly is closely correlated to the building and underground structure corrections, as the error on these corrections is spatially variable and linearly related to the magnitude of the corrections (eq. 2). Furthermore, the magnitude of this error is locally dominant compared to the error on the other contributions (eq. 1), when stations are close to underground structures or buildings, with associated important corrections (Figure 3). This error reaches at most 0.04 mGal in the direct vicinity of the four level underground parking lot located in the centre of the study area. In regions of low building and underground structure corrections, and for stations at a distance from buildings and cavities, the error on the Bouguer anomaly is dominated by the error on the gravity measurements.

3.5 Residual anomaly significance threshold

To be considered significant, anomalous zones within the residual anomaly map must have a magnitude larger than twice the error on the Bouguer anomaly (see section 3.4). This is akin to a 95 % confidence level, had the error been of Gaussian nature (white noise), which is however not the case as the error is spatially correlated due to the building and underground structures corrections errors.

The significance threshold map (Figure 6) is thus computed as twice the error on the Bouguer anomaly. It is largely correlated to the building and underground structure correction map (compare Figure 6 to Figure 3), as the errors on these corrections are the dominant contributors to the error on the Bouguer

anomaly, in the direct vicinity of buildings and underground structures. The threshold reaches 0.08 mGal near the four level underground parking lot.

At a distance from buildings and underground structures, the significance threshold is dominated by the gravity measurement error, which is dependent on the different gravity meters used during the three phases of the study (see Figure 1 and Table 1). The significance threshold reaches values as low as 0.012 mGal for phase 3 measurements due to good reproducibility of the meter used.

Therefore, in order to be considered significant, a gravity anomaly will need to be of much larger magnitude near buildings and underground structures, where the significance threshold is higher, than at a distance from the buildings and underground structures, where the significance threshold is lower. This means that cavities must be of larger dimensions and shallower near buildings and underground structures as compared to further away from them, in order to be detected with confidence. Although outside the scope of the present paper, a parametric study could be performed to determine at what distance from buildings and known underground structures, target cavities of different sizes and depths may be significantly detected as a function of the constitutive elements of the significance threshold determination. Near buildings and caves, the latter is dominated by errors on the anthropogenic corrections, which are related to building dimensions and underground structures dimensions and depth. These parameters should greatly affect the result of the afore-mentioned parametric study.

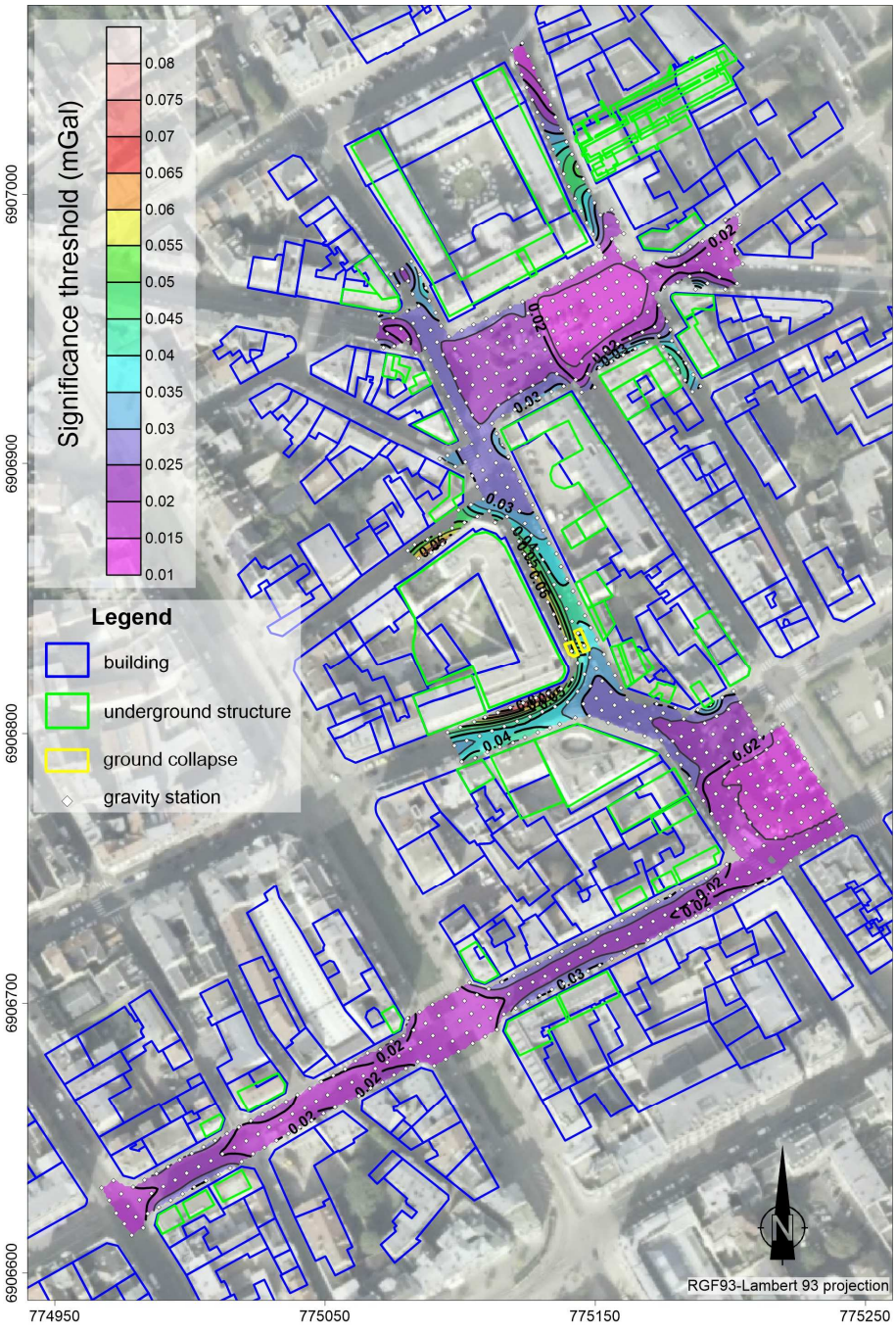

Figure 6: significance threshold (mGal) of the residual anomaly map

3.6 Residual anomaly map

The residual anomaly map (Figure 7) ranges between -0.057 mGal and 0.027 mGal. In this study, our focus is on negative anomalies, which mark low-density zones. Negative anomalies are considered significant if their magnitude is larger than the significance threshold (Figure 6) on at least two or more

contiguous stations. The latter condition is set to prevent that a single outlier measurement is considered significant. Under these conditions, we identify 12 significant anomalies, named A1 to A12 (Figure 7).

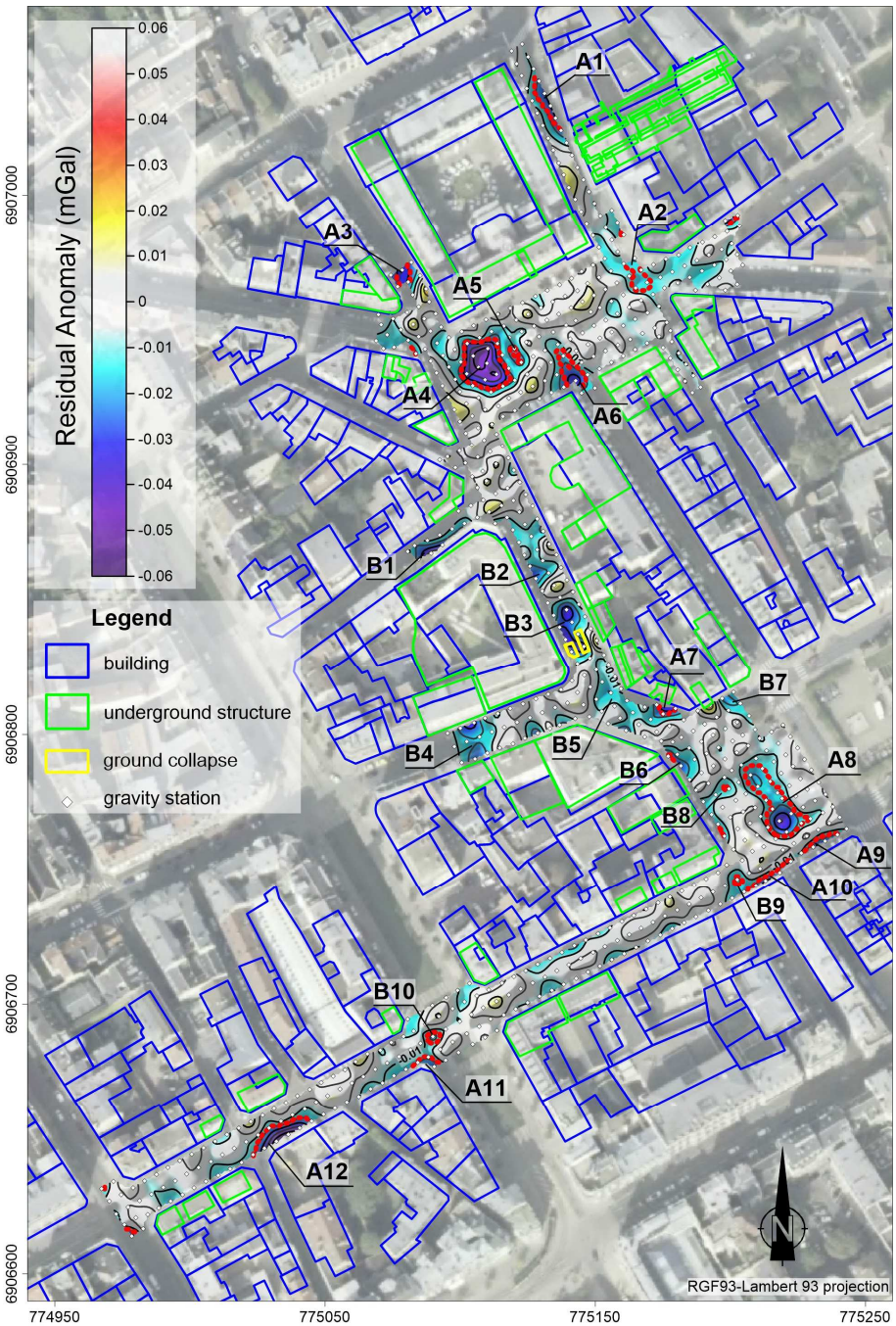

Figure 7: Residual anomaly map (mGal), iso contours are every 0.01 mGals. Dashed red lines delimit significant anomalies, named A1 to A12. Anomalies B1 to B10 are also considered.

The highest magnitude anomaly, A4, reaching -0.057 mGal, also has the largest footprint, is fully delimited and is located on the City Hall plaza. Anomaly A8 is also notable because it is fully delimited,

it has a significant footprint, and it reaches -0.040 mGal magnitude. Anomaly A5 is also fully delimited but of limited footprint and magnitude. No other significant anomalies are fully delimited, being located on the borders of the gravity survey coverage. Notably, anomalies A1, A9, A10, A11 and A12 develop towards buildings where suspected underground structures exist, but wherein no access was granted to measure the dimensions of the cellars. Therefore, it is reasonable to associate these anomalies to the suspected but uncorrected underground structures.

Anomalies A2, A3, A6 and A7 are also not fully delimited, and cannot be associated to uncorrected cellars underneath nearby buildings, as the cellars in nearby buildings are corrected.

Although not meeting the conditions above described to be labelled significant, we consider 10 further anomalies, named B1 to B10. Such anomalies are deemed noteworthy if their magnitude is larger than 0.020 mGals in regions of high significance threshold (Figure 6), or if a single station is significant, and located within a negative zone, or close to a significant anomaly.

Anomalies B1 to B5 are located within a high significance threshold region, due to the important corrections associated with the four level parking lot. Anomaly B3 is noteworthy as it is in the immediate vicinity of the collapse footprints (the collapses were filled at the time of the surveys) and is developed to the NW of the collapses. Anomalies B6 and B7 seem to be developing towards nearby buildings, and anomalies B9 and B10 are single-station significant anomalies, located near significant anomalies A10 and A11.

4. Discussion

4.1 Recommendations based on the gravity residual anomaly map

Gravity anomalies cannot be uniquely interpreted, as there is an infinite number of depth-dimension-density contrast solutions that may account for a given anomaly. We acknowledge that multiple methods exist to evaluate the depth of targets from potential fields, through Euler deconvolution(Murdie et al., 1999; Thompson, 1982), direct modelling (Martinez-Moreno et al., 2016), inverse modelling and other methods (see Fedi & Pilkington (2012) for a comprehensive review).

It is therefore good practice to systematically recommend one or more drill holes located on or near the apexes of negative anomalies, to verify their nature and the presence of cavities. If a drill hole does not

reveal an anomalous zone, it is also good practice to repeat the drill hole with a position translated a couple of meters. This is motivated by the fact that when two cavities are close together; the resulting gravity signal is coalescent, showing a minimum located between the cavities. In such cases, a borehole located on the anomaly's apex will not encounter the cavities, and this warrants additional holes to be drilled.

Based on the identified residual anomalies, BRGM recommended that every notable anomaly should be drilled to a depth of 15 m, using destructive rotary instrumented drilling, with recordings of torque, down-thrust, penetration rate and mud pressure. The 15 m depth is based on the local knowledge of cavities in Reims city centre, as the vast majority of known cavities lie above that depth (Thuon, 2010). High penetration rate and low thrust parameters anomalous zones are proxies for cavities (Pfister, 1985). Downhole camera inspections were further recommended if anomalous zones are evidenced in the borehole, to ascertain their nature.

In total, twenty-three borehole sites were recommended, 13 of which were classified as priority 1 borehole sites, and the remaining 10 as priority 2 (Figure 8). Priority 1 borehole sites were positioned within significant anomalies that are mostly circumscribed, and within anomalies that are close to the collapses (D11 in B3, and D12 in B5). Priority 2 borehole sites were positioned within significant anomalies whose origin are suspected to be linked with uncorrected cellars (boreholes D7, D8 and D22, D23 within anomalies A1 and A12). It was recommended that these boreholes should be drilled if no evidence of a cellar was found below the neighbouring buildings.

Furthermore, additional priority 2 drill holes were positioned within anomalies not reaching the significance threshold. These boreholes were to be drilled if nearby boreholes detect cavities and that reasonable doubt existed on the presence of a cavity.

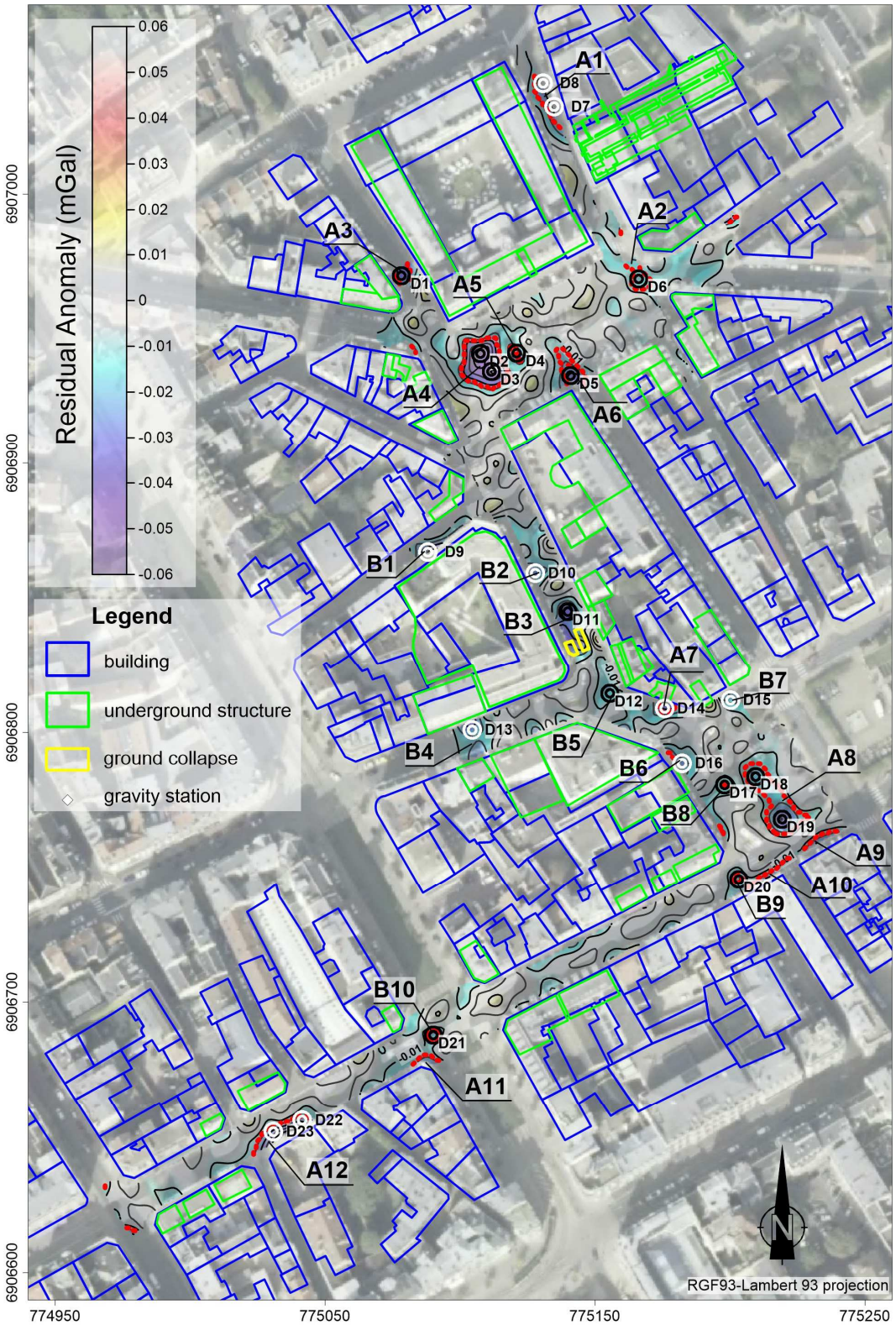

Figure 8: Recommended drill holes locations, noted D1 to D23. Black circles represent priority 1 drill holes, white circles priority 2 drill holes.

4.2 Drill hole results

Out of the 13 priority 1 recommended drill holes (Figure 8), only 5 were drilled: D2, D3, D4, D5 and D11 (GingerCEBTP, 2016), located on anomalies A4, A5, A6 and B3. These drill holes did not go through an empty cavity, but encountered 5 to 7 meters of very un-compacted fill overlying the chalk, characterized by high penetration rates. Following BRGM recommendations, a further hole was drilled between D2 and D3 and a two-level vaulted cellar was encountered, between depths of 2.1 m and 3.8 m for the first level, and depths of 4.8 and 6.8 m for the second level (Figure 9). This highlights the importance of drilling multiple holes per anomaly, to maximize the odds of encountering a potential cavity.

Downhole camera inspection allowed determining that both cellars were partially filled with rubble and sandy material, attesting the presence of previous collapses. Both cellars are approximately 10 m by 5 m in footprint, and 2 m high, yet the precise dimensions and orientation were not communicated to us.

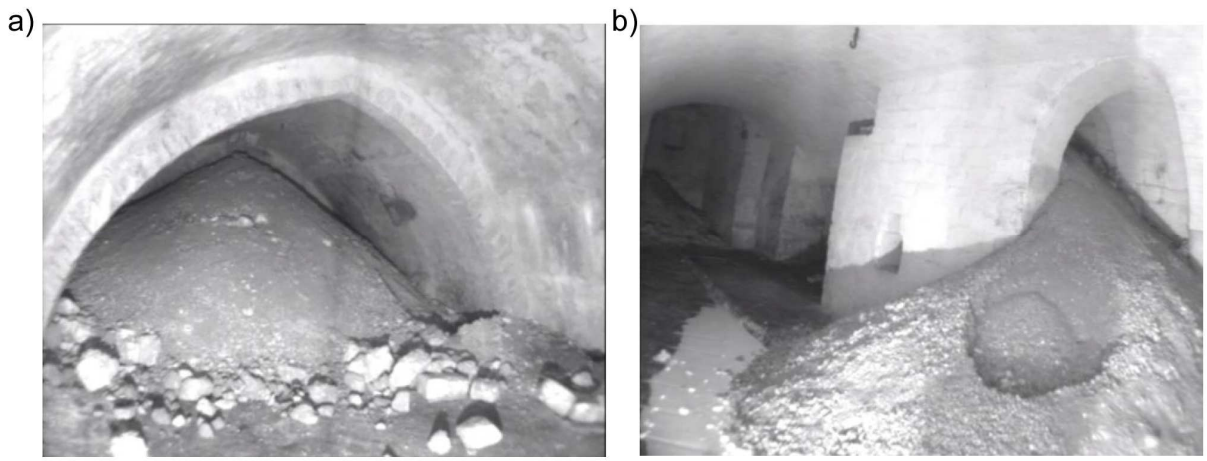

Figure 9 Screenshots from downhole camera footage for a) upper level cellar and b) lower level cellar, after GingerCEBTP (2016)

Once we obtain the precise topographical data of the two-level cavity, it will be insightful to model its gravity effect and compare it with the measured gravity anomaly. By examining the differences between observed and modelled gravity anomalies, one could determine if the discovered cavity accounts entirely for the observed signal, and if there are leftover anomalies that might be due to adjacent low-density zones, such as un-compacted fill volumes or cavities.

The City of Reims decided to safeguard the discovered cellar for future generations and not destroy it or fill it. Its presence was thus taken into account in the recent renovation of the City Hall plaza: the area above the cavity was reclassified as a pedestrian only zone. This in effect reduces the collapse hazard by decreasing the loads applied on the surface.

5. Conclusions

Microgravity surveying was carried out in a highly urbanized city centre setting in Reims, France, to detect undocumented cavities below ground, following the occurrence of two ground collapses affecting a busy street. In this context, surrounding buildings and underground structures constitute respectively excess mass above, and deficit mass below the gravimeter, which result in negative gravity anomalies. These anomalies may have magnitudes comparable to or larger than the target signal, hence obscuring its detection.

Furthermore, hundreds of buildings and underground structures surround the gravity stations, which calls for simplifying assumptions for their correction.

For buildings, we make the following simplifying assumptions: mass is concentrated on the outer walls, and only a limited number of parameters, such as footprint, height, wall thickness and density are required. We opt for line mass approximation to model the walls. Underground structures are approximated and modelled as flat-top polygonal structures, which requires their footprint, depth and dimensions.

Our correction scheme is effective, as important border anomalies in the uncorrected Bouguer anomaly are mitigated and no longer visible in the corrected Bouguer anomaly. In effect, these corrections make the Bouguer anomaly more straightforward to interpret, which facilitates the determination of a regional anomaly, and ultimately leads to a more meaningful residual anomaly. We also present an error budget estimate, in which errors in the anthropogenic corrections are approximated. This allows us to establish a significance threshold, which is used to delineate significant anomalies.

A number of significant anomalies were found, and drill holes were recommended to control the anomalies and check for cavities. A two level cellar was found in the middle of City Hall Plaza, under anomaly A4. Other drillholes found un-compacted fill material.

The methodology presented in this case study may be used for gravity of microgravity surveys located in highly-urbanised areas, i.e. in city centres near hundreds of buildings and known underground structures. For surveys located within or in the immediate vicinity of massive buildings with complex architectures, such as churches, we recommend that more advanced building corrections schemes should be used (Panisova et al., 2013; Panisova et al., 2016; Panisova et al., 2012).

A promising approach to better correct the gravity effect of both existing cavities and buildings is to survey them using a portable handheld laser-scanning device, which allows for fast and precise point cloud generation (Dewez et al., 2017). Using this method, the error on the anthropogenic corrections should be lowered, which in turn should lower the significance threshold near buildings and known underground structures. This should allow for detecting cavities with more confidence in these regions of strong corrections.

6. Acknowledgements

This study was jointly funded by the Communauté Urbaine du Grand Reims and by BRGM, under projects CF16CHA068, CF16CHA093 and CF16CHA094.

The writing time for this paper was supported BRGM research grant RP18DRP011.

We are indebted to T. Prunet for his precious help in the field during the geophysical campaigns.

We wish to thank the editor M. Fedi, R. Pasteka and an anonymous reviewer for their constructive comments, which greatly enhanced this manuscript.

7. References

Bishop, I., Styles, P., Emsley, S.J. and Ferguson, N.S., 1997. The detection of cavities using the microgravity technique: case histories from mining and karstic environments. Geological Society, London, Engineering Geology Special Publications, 12(1): 153-166.

Blížkovský, M., 1979. Processing and applications in microgravity surveys. Geophysical Prospecting, 27(4): 848-861.

Boddice, D., Atkins, P., Rodgers, A., Metje, N., Goncharenko, Y. and Chapman, D., 2018. A novel approach to reduce environmental noise in microgravity measurements using a Scintrex CG5. Journal of Applied Geophysics, 152: 221-235.

Bott, M.H., 1959. The use of electronic digital computors for the evaluation of gravimetric terrain corrections. Geophysical Prospecting, 7(1): 45-54.

Butler, D.K., 1984. Microgravimetric and gravity gradient techniques for detection of subsurface cavities. Geophysics, 49(7): 1084-1096.

Castiello, G., Florio, G., Grimaldi, M. and Fedi, M., 2010. Enhanced methods for interpreting microgravity anomalies in urban areas. first break, 28(8).

Chromčák, J., Grinč, M., Pánisová, J., Vajda, P. and Kubová, A., 2016. Validation of sensitivity and reliability of GPR and microgravity detection of underground cavities in complex urban settings: Test case of a cellar. Contributions to Geophysics and Geodesy, 46(1): 13-32.

D'Errico, J., 2005. Surface fitting using gridfit. MATLAB Central File Exchange.

Debeglia, N. and Dupont, F., 2002. Some critical factors for engineering and environmental microgravity investigations. Journal of Applied Geophysics, 50(4): 435-454.

Dewez, T.J.B., Yart, S., Thuon, Y., Pannet, P. and Plat, E., 2017. Towards cavity collapse hazard maps with Zeb-Revo handheld laser scanner point clouds. The Photogrammetric Record, 32(160): 354-376.

Dilalos, S., Alexopoulos, J.D. and Tsatsaris, A., 2018. Calculation of Building Correction for urban gravity surveys. A case study of Athens metropolis (Greece). Journal of Applied Geophysics, 159: 540-552.

Fais, S., Radogna, P.V., Romoli, E., Matta, P. and Klingele, E.E., 2015. Microgravity for detecting cavities in an archaeological site in Sardinia (Italy). Near Surface Geophysics, 13(5): 495-502.

Fajklewicz, Z.J., 1976. Gravity vertical gradient measurements for the detection of small geologic and anthropogenic forms. Geophysics, 41(5): 1016-1030.

Fedi, M. and Pilkington, M., 2012. Understanding imaging methods for potential field data. Geophysics, 77(1): G13-G24.

Flury, J., Peters, T., Schmeer, M., Timmen, L., Wilmes, H. and Falk, R., 2007. Precision gravimetry in the new Zugspitze gravity meter calibration system. Harita Dergisi, 18: 401-406.

Fores, B., Champollion, C., Le Moigne, N. and Chery, J., 2017. Impact of ambient temperature on spring-based relative gravimeter measurements. Journal of Geodesy, 91(3): 269-277.

GingerCEBTP, 2016. Compte rendu : Reconnaissance des anomalies gravimétriques. NRE2.G.128.41.

Jamal, 2014. RegularizeData3D. MATLAB Central File Exchange.

Leucci, G. and De Giorgi, L., 2010. Microgravimetric and ground penetrating radar geophysical methods to map the shallow karstic cavities network in a coastal area (Marina Di Capilungo, Lecce, Italy). Exploration Geophysics, 41(2): 178-188.

Loj, M. and Porzucek, S., 2019. Detailed analysis of the gravitational effects caused by the buildings in microgravity survey. Acta Geophysica, 67(6): 1799-1807.

Longman, I.M., 1959. Formulas for computing the tidal accelerations due to the moon and the sun. Journal of Geophysical Research, 64(12): 2351-2355.

Martinez-Moreno, F.J., Galindo-Zaldivar, J., Gonzalez-Castillo, L. and Azanon, J.M., 2016. Collapse susceptibility map in abandoned mining areas by microgravity survey: a case study in Candado hill (Malaga, southern Spain). Journal of Applied Geophysics, 130: 101-109.

Martínez-Moreno, F.J., Pedrera, A., Ruano, P., Galindo-Zaldívar, J., Martos-Rosillo, S., González-Castillo, L., Sánchez-Úbeda, J.P. and Marín-Lechado, C., 2013. Combined microgravity,

electrical resistivity tomography and induced polarization to detect deeply buried caves: Algaidilla cave (Southern Spain). Engineering Geology, 162: 67-78.
Mochales, T., Casas, A.M., Pueyo, E.L., Pueyo, O., Román, M.T., Pocoví, A., Soriano, M.A. and Ansón, D., 2008. Detection of underground cavities by combining gravity, magnetic and ground penetrating radar surveys: a case study from the Zaragoza area, NE Spain. Environmental Geology, 53(5): 1067-1077.
Moreau, C., 2008. Vieillissement naturel en milieu urbain de pierres calcaires hydrofugées: Evaluation de la durabilité des traitements et de leur impact sur le nettoyage, Reims.
Moritz, H., 1980. Geodetic reference system 1980. Journal of Geodesy, 54(3): 395-405.
Murdie, R.E., Styles, P., Upton, P., Eardley, P. and Cassidy, N.J., 1999. Euler deconvolution methods used to determine the depth to archaeological features. Geological Society, London, Special Publications, 165(1): 35-40.
Murthy, I.V.R. and Swamy, K.V., 1996. Gravity anomalies of a vertical cylinder of polygonal cross-section and their inversion. Computers & Geosciences, 22(6): 625-630.
Nagy, D., 1966. The prism method for terrain corrections using digital computers. pure and applied geophysics, 63(1): 31-39.
Nowell, D.A.G., 1999. Gravity terrain corrections - an overview. Journal of Applied Geophysics, 42(2): 117-134.
Omnes, G., 1977. High accuracy gravity applied to the detection of karstic cavities. Karst hydrogeology: International Association of Hydrogeology Memoir, 12: 273-284.
Panisova, J., Fraštia, M., Wunderlich, T., Pašteka, R. and Kušnirák, D., 2013. Microgravity and Ground-penetrating Radar Investigations of Subsurface Features at the St Catherine's Monastery, Slovakia. Archaeological Prospection, 20(3): 163-174.
Panisova, J., Murin, I., Pašteka, R., Haličková, J., Brunčák, P., Pohanka, V., Papčo, J. and Milo, P., 2016. Geophysical fingerprints of shallow cultural structures from microgravity and GPR measurements in the Church of St. George, Svätý Jur, Slovakia. Journal of Applied Geophysics, 127: 102-111.
Panisova, J., Pašteka, R., Papco, J. and Fraštia, M., 2012. The calculation of building corrections in microgravity surveys using close range photogrammetry. Near Surface Geophysics, 10(5): 391-399.
Pfister, P., 1985. Recording drilling parameters in ground engineering. Ground Engineering: pp. 16-21.
Radogna, P.V., Olivier, R. and Logean, P., 2003. Micro-gravity survey in urban environment: modelling, evaluation and correction of buildings influence, 9th EAGE/EEGS Meeting.
Repanić, M. and Kuhar, M., 2018. Modelling hysteresis effect in Scintrex Cg-3m gravity readings. Geophysical Prospecting, 66(1): 257-269.
Reudink, R., Klees, R., Francis, O., Kusche, J., Schlesinger, R., Shabanloui, A., Sneeuw, N. and Timmen, L., 2014. High tilt susceptibility of the Scintrex CG-5 relative gravimeters. Journal of Geodesy, 88(6): 617-622.
Styles, P., Toon, S., Thomas, E. and Skittrall, M., 2006. Microgravity as a tool for the detection, characterization and prediction of geohazard posed by abandoned mining cavities. First Break, 24(5): 51-60.
Thompson, D.T., 1982. EULDPH: A new technique for making computer-assisted depth estimates from magnetic data. Geophysics, 47(1): 31-37.
Thuon, Y., 2010. Inventaire des cavités souterraines (hors mine) du département de la Marne (51). Rapport final. BRGM/RP-59361-FR.
Vilain, L., 2016. Mais pourquoi le sol se dérobe sous nos pieds à Reims ?, https://france3-regions.francetvinfo.fr/grand-est/marne/reims-metropole/reims/pourquoi-sol-se-derobe-nos-pieds-reims-1029215.html. (accessed 29 November 2018).
Yu, D., 2014. The Influence of Buildings on Urban Gravity Surveys. Journal of Environmental and Engineering Geophysics, 19(3): 157-164.